arXiv:cond-mat/0102095v8 [cond-mat.mes-hall] 2 Apr 2002

Scattering phase shifts in quasi-one-dimension

P. Singha Deo and Swarnali Bandopadhyay
S.N. Bose National Centre for Basic Sciences, J.D.Block, Sector III, Salt Lake City, Calcutta 700098, India

Sourin Das
Harish Chandra Research Institute, Chhatnag Road, Jhusi, Allahabad 211019, India
(February 1, 2008)

Scattering of an electron in quasi-one dimensional quantum wires have many unusual features, not found in one, two or three dimensions. In this work we analyze the scattering phase shifts due to an impurity in a multi-channel quantum wire with special emphasis on negative slopes in the scattering phase shift versus incident energy curves and the Wigner delay time. Although at first sight, the large number of scattering matrix elements show phase shifts of different character and nature, it is possible to see some pattern and understand these features. The behavior of scattering phase shifts in one-dimension can be seen as a special case of these features observed in quasi-one-dimensions. The negative slopes can occur at any arbitrary energy and Friedel sum rule is completely violated in quasi-one-dimension at any arbitrary energy and any arbitrary regime. This is in contrast to one, two or three dimensions where such negative slopes and violation of Friedel sum rule happen only at low energy where the incident electron feels the potential very strongly (i.e., there is a very well defined regime, the WKB regime, where FSR works very well). There are some novel behavior of scattering phase shifts at the critical energies where S-matrix changes dimension.

PACS: 73.23.-b, 72.10.-d, 72.10.Bg

I. INTRODUCTION

Elastic scattering in one, two and three dimensions is well understood [1]. In a scattering process there are some important physical quantities like scattering amplitude and scattering phase shift. While the scattering intensity is directly related to the scattering amplitude, the scattering phase shifts are also very important physical quantities and the Friedel-sum-rule (FSR) relates them to the density of states (DOS).

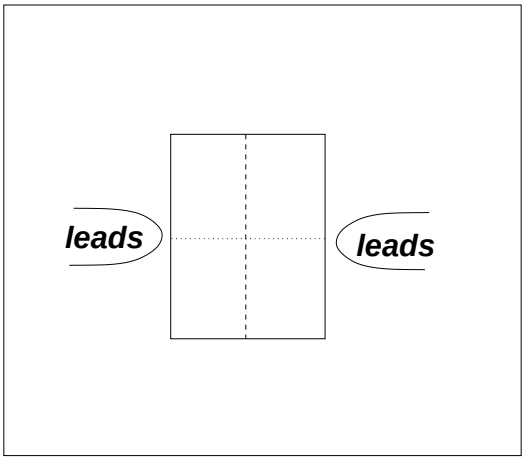

FIG. 1. A rectangular quantum biliard or quantum dot, weakly coupled to leads. The dotted line is along the x-axis and the dashed line is along the y-axis.

At low temperatures, inelastic collisions are greatly suppressed. As a result the phase coherence length of an electron can become a few microns. Mesoscopic systems are defined as systems in which the phase coherence length exceeds the sample size. In such a system elastic scattering is the dominant feature and such mesoscopic samples can be understood as phase coherent elastic scatterers. With the experimental realizations of mesoscopic systems and their possibility of being applied in nanotechnology and quantum computing, understanding scattering effects in quasi-one dimensions (Q1D) has also become important at present. This is also essential because the Landauer conductance formula relates the conductance to partial scattering intensities and also one can now probe scattering phase shift directly in an experiment [2–4]. Mesoscopic samples are normally made up of metals or semiconductors, and the defects in them are generally point defects. Hence we will restrict our analysis to delta function potential impurities.

Recently a new kind of scattering phase shift was discussed in Q1D, in connection with the violation of the parity effect [5]. To explain this phase shift and the violation of parity effect, here we elaborate some portions of Ref. [5] and explain what are symmetry dictated nodes (SDN) and non-symmetry dictated nodes (NSDN) that can arise in a Q1D system. For example let us consider a rectangular quantum biliard or dot connected to leads by quantum mechanical tunneling as shown in Fig.1. The system has reflection symmetry across the x-axis as well as the y-axis. Also the x-y components separate and spanning nodes (nodes that span across the direction of propagation and shown by dashed line in Fig.1) as well

as non-spanning nodes (shown by dotted line in Fig.1) develop in the geometry, dictated by the reflection symmetries. There are various symmetries that give rise to nodes in the wave-function and we call them SDN (for example the antisymmetric property of the many body wave function result in nodes). But if quantum coherence extends to some distance inside the leads then one can model the phase coherent quantum dot as shown in Fig.2.

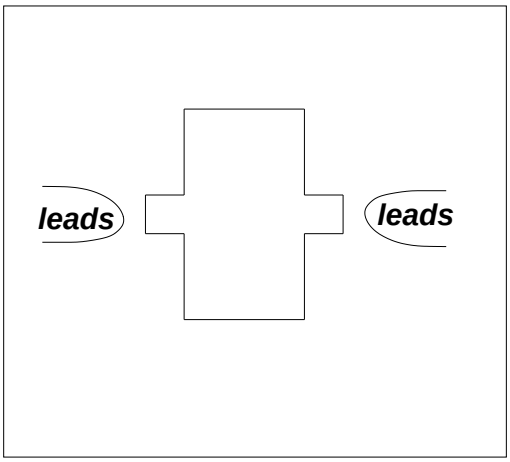

FIG. 2. A more realistic model of the quantum dot of Fig.1.

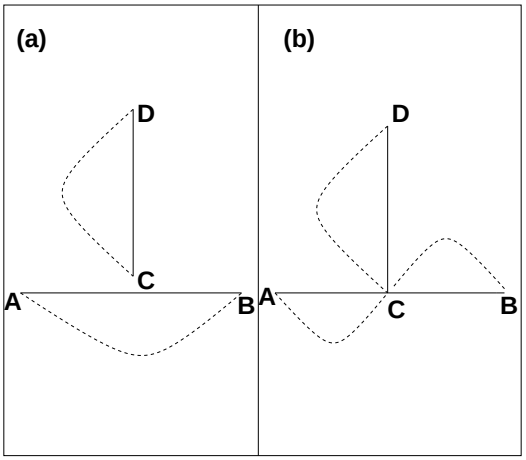

FIG. 3. Two one dimensional quantum wires of equal lengths, AB and CD, shown by solid lines, placed along x and y directions, respectively. The origin (x=0, y=0) is at the mid-point of AB. (a) CD is not connected to AB. (b) CD is connected to AB.

Note that in this case also reflection-symmetry holds in the x-direction as well as in the y-direction, but x-y components do not separate. So by tuning the boundary condition in y-direction by a gate voltage one can develop nodes that try to develop across y-direction but also act across x-direction and change the phase of the wave function in x-direction by π. We call them NSDN because they do not originate due to the symmetry of the Hamiltonian. There are many configurations of such NSDN [6], the simplest one was discussed for the stub geometry (shown in Fig.3) in ref. [5].

Consider for example two finite one dimensional quantum wires of equal length, AB and CD placed perpendicular to each other as shown in Fig.3 by the solid lines. When CD is completely detached from AB as shown in Fig.3(a), then the quantum mechanical wave function in AB and CD in the ground state is shown by the dotted lines. They are basically the ground state wave function in an infinite potential well in one dimension (1D). As is known to us, the ground state wave functions are by symmetry, even parity states without any nodes, except at the boundary. But when CD is attached to AB to give a T-shaped stub structure as shown in Fig.3(b), then CD forms a node at C, which is also the midpoint of AB. The wave function in this case is again shown by dotted lines and the wave function between A and B is no longer an even parity state but an odd parity state. The node at C between A and B does not originate from the symmetry of the Hamiltonian and is not a symmetry dictated node (SDN). It is rather forced by the boundary condition in the y-direction and is a NSDN. An infinitesimal change in the length CD makes this node disappear and then we have no node between A and B. The node at C induces a phase change by π and when we join A and B together to form a ring-stub system, we also get persistent currents without parity effect, as parity of the persistent currents is sensitive to the number of nodes in the wave function [7].

Fano resonances [8] are a very general feature of Q1D [9–11] systems in the presence of defects and the Fano resonances are characterized by a zero-pole pair of the transmission amplitude in the complex energy plane. When semi infinite leads are attached to A and B in Fig.3(b) then the transmission amplitude of the stub structure also has zero-pole pair and one gets Fano resonances [10]. At the energy corresponding to the pole a charge gets trapped by the scatterer and there is also an energy when there is a zero transmission across the scatterer. At the energy corresponding to the zero, scattering phase shift discontinuously changes by π due to the NSDN [5].

It seems at present that this phase due to NSDN is necessary to understand the experimental results of Refs. [2–4]. Initial analysis of the experiments in terms of Friedel-sum-rule [12] revealed the shortcomings of applying Friedel-sum-rule to the quantum dot. The phase change due to NSDN can explain the experimental data was first proposed in Ref. [13] and later discussed in Refs. [11,14–18].

The Friedel-sum-rule (FSR) can be stated as [19]

$$\theta(E_2) - \theta(E_1) \approx \pi N(E_2, E_1). \quad (1)$$

In 1D, 2D and 3D, the equality is known to be approximate, and is almost exact in the WKB regime where generally transport occurs. Here $N(E_2, E_1)$ is the variation in the number of states in the energy interval $[E_1, E_2]$ due to the scatterer and [20]

$$\theta = \frac{1}{2}\sum \xi_i = \frac{1}{2i} ln(det[S]), \tag{2}$$

S being an n×n scattering matrix and $e^{i\xi_i}$, i=1,2,....n are the n eigenvalues of the unitary matrix S. In differential form the FSR can also be stated as

$$\frac{\partial\theta}{\partial E} = \frac{1}{2i}\frac{\partial}{\partial E} ln(det[S]) \approx \pi(\rho(E) - \rho_0(E)), \tag{3}$$

where $(\rho(E) - \rho_0(E))$ is the variation of the DOS or the difference in the DOS due to the presence of the potential. $\rho(E)$ and $\rho_0(E)$ can be found by integrating the local DOS $\rho(x, y, z, E)$ and $\rho_0(x, y, z, E))$ which are related to the electron probability. However, if FSR is to be useful in mesoscopic systems where scattering phase shifts can be accurately measured, and where we are always interested to study a finite region of space, then we must see to what extent it can give the local DOS. In fact in 1D, 2D or 3D it does so extremely well and so we ask the question that how good it is in Q1D. We shall show that in Q1D, FSR will fail to give the local DOS as well as the global DOS at all energy regimes.

For a symmetric scatterer in a strictly 1D system when transmission and reflection amplitudes are denoted by t and r, respectively,

$$S = \begin{pmatrix} r & t \\ t & r \end{pmatrix}.$$

In this case, one can show [17]

$$\frac{\partial\theta}{\partial E} = \frac{\partial arg(t)}{\partial E}, \tag{4}$$

which means sum of the phases of the eigen values of S is equal to the phase of some particular matrix element of S.

But now we know that in systems that are not strictly 1D, one can have zero-pole pairs and then Eq.(4) is not valid because of the π phase shifts induced by NSDN. Note that for the system in Fig.3(b), although the scattering matrix is 2×2, the point C is connected to 3 directions and is hence a Q1D system. A quantum wire with a finite width and only one propagating channel [11] also is a Q1D system with a 2×2 scattering matrix. For such systems, that are not strictly one dimensional but has a 2×2 scattering matrix

$$\frac{\partial\theta}{\partial E} \neq \frac{\partial arg(t)}{\partial E} \tag{5}$$

but

$$\frac{\partial\theta}{\partial E} \approx \pi(\rho(E) - \rho_0(E)), \tag{6}$$

i.e., when we go from 1D (with 2x2 S matrix) to Q1D (also with 2x2 S matrix) then Eq. (3) holds but Eq. (4) does not hold. This analysis was presented by Lee [16] and by Büttiker and Taniguchi [17]. Their analysis is restricted to the system in Fig.3(b) and S-matrices that are 2×2. Eq.(3) is not violated in the presence of NSDN and π phase slips because $det[S] = r^2 - t^2$ and if $arg(t)$ changes by π then $[arg(t^2)]$ changes by 2π or 0 and hence $det[S]$ is unaffected by the π phase slips. Thus for such a single propagating channel this phase shift is well understood by now. It has been emphasized that the multi-channel case also needs to be studied [18], specially since scattering phase shifts can now be probed experimentally in the single channel case [2,3] as well as in the multi-channel case [4], but no such study has been reported so far.

In particular, the FSR is very important in condensed matter Physics, because from the scattering phase shift (that can be determined experimentally) one can know the local DOS inside a disordered sample without knowing its internal details. Even theoretically, except in very simple situations, the wave function inside the scatterer has infinite degrees of freedom and exact calculation of local DOS from the exact wave function inside the scatterer may be non-trivial. While a good estimate of local DOS from the S-matrix, which is on its own a very useful quantity, can greatly reduce the complexities. In this work we will study the n channel scattering problem in a Q1D quantum wire, with special emphasis on FSR and Wigner delay time [21,22]. Refs. [16] and [17] parameterize the S-matrix in a particular way (there are in fact many different ways of parameterizing the S-matrix) in which the scattering matrix elements become independent of energy. We will show that this energy dependence, that are not important in 1D play a very crucial role in Q1D multi-channel scattering. Hence in section II we will generalize the work of Refs. [16] and [17] for real energy dependent 2×2 scattering matrices. The n channel case will be analyzed in section III and IV. In section V we will show some novel phase shifts at critical energies where S matrix changes dimensions. Section VI is devoted to conclusions.

II. SCATTERING IN ONE-DIMENSION AND NEGATIVE VALUES OF $D\theta/DE$

In Fig.4 we consider a potential that is described in details in the figure caption. The quantum mechanical wave function or the solution to the Schrödinger equation in different regions is also shown and explained in the figure and its caption. We will always normalize the incoming wave-function such that its amplitude is 1. Griffiths boundary conditions for this system gives the following equations [23,24] (we use $2m = 1$ and $\hbar = 1$).

$$1 + r = a + b, \tag{7}$$

$$ae^{ikl} + be^{-ikl} = t, \tag{8}$$

$$ik(1-r) - ik(a-b) = -V(1+r) \quad \text{and} \tag{9}$$

$$ik(ae^{ikl} - be^{-ikl}) - ikt = -V(ae^{ikl} + be^{-ikl}). \tag{10}$$

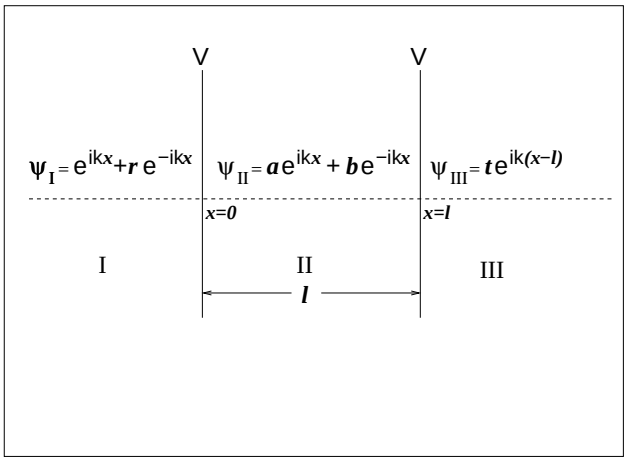

FIG. 4. Two identical delta function potentials separated by a length l. Strength of each potential is V. The thick vertical lines denote the positions of the potentials and the thin horizontal line is the direction of propagation. A plane wave of unit amplitude is incident from the left and wave function in different regions (marked as I, II and III) is written down in the figure. r and t are the reflection and transmission amplitudes, respectively, of the entire system and $k = \sqrt{E}$ is the incident wave vector. The origin of coordinates is shown in the figure.

We will first analyze this system in detail and generalize the results of Refs. [16,17] further by considering realistic energy dependent r and t, that will later help us to accentuate the new features that can be observed in a multi-channel disordered quantum wire.

First of all let us calculate the local DOS and global DOS to see how much it agrees with $d\theta/dE$. Although the basic facts discussed in this section is known in the Greens function formalism, to the best of our knowledge, quantitative disagreement (or agreement) has not been shown so far. Using quantum mechanical expression for the local DOS integrated over the region II in Fig. 4, i.e.,

$$\rho_R = \frac{2}{hv}\int_0^l \mid ae^{ikx} + be^{-ikx} \mid^2 dx,$$

it is easy to show from Eq. 3 that (the Eq. below is consistent with Ref. [17] and some hints on its derivation is given in Ref [25])

$$\frac{d\theta}{d(kl)} \approx \bar{\rho} + \frac{\rho_q}{l} = \rho' \quad \text{(say)}, \tag{11}$$

$$\text{where} \quad \bar{\rho} = \mid a \mid^2 + \mid b \mid^2 \text{ and} \tag{12}$$

$$\rho_q = \int_0^l \left(ab^* e^{2ikx} + ba^* e^{-2ikx}\right) dx. \tag{13}$$

Here $\frac{\rho_q}{l}$ is a term that arises because of quantum mechanical interference and it can be seen that the integrand in Eq.(13) oscillates with x. For $|\frac{E}{V}| > 1$ (this is the WKB regime when the electron does not feel the potential strongly and is almost entirely transmitted) $\frac{\rho_q}{l}$ is negligibly small. This is shown in Fig.5, where we plot $\rho^{'}$ (the dashed curve) and $\bar{\rho}$ (the dotted curve). The two curves are almost the same for $|\frac{E}{V}| > 1$, which means $\frac{\rho_q}{l}$, being the difference between the dashed and dotted curves is vanishingly small above this energy. It is known that to get the equality between the LHS and RHS of Eq. 11, it is necessary to drop the term $\frac{\rho_q}{l}$ [26]. It is also known that this deviation arises because we are considering the local DOS rather than the global DOS. If we consider the global DOS, i.e.,

$$\rho(E) = \frac{2}{hv}\int_{-\infty}^{\infty} \psi^*(x)\psi(x)dx$$

where $\psi(x)$ is the quantum mechanical wavefunction at x, then instead of Eq. (11) we get

$$\frac{d\theta}{d(kl)} \approx Lt_{l\to\infty}(|a|^2 + |b|^2).$$

The equality is still approximate although almost exact in the WKB regime because the RHS is positive definite, while it is well known that the LHS can become negative at low energy (non-WKB regime) as will be demonstrated below. To get the equality it is necessary to neglect something else as we shall soon see. This second thing that we shall drop is however not due to the fact that we are considering the local DOS. It is an inherent approximation of the FSR even when we are considering the global DOS and hence also when we are considering the local DOS. The ρ_q/l term or the interference term inside the scatterer does not arise in the case when $l \to 0$ as in the case to be considered in section IV. All the deviation to be observed there is due to this inherent weakness of the FSR. We shall also see below that this inherent weakness of the FSR is negligible in 1D, 2D or 3D but becomes very formidable in quasi 1D.

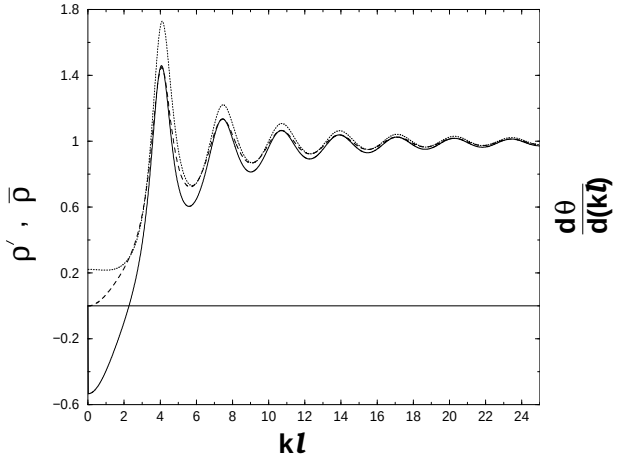

FIG. 5. The system under consideration is shown in Fig.4. The solid curve gives the exact $d\theta/d(kl)$, the dashed curve gives the $\rho^{'}$ and the dotted curve gives $\bar{\rho}$. This plot is done for $Vl^2 = -5, \hbar = 1, 2m = 1$.

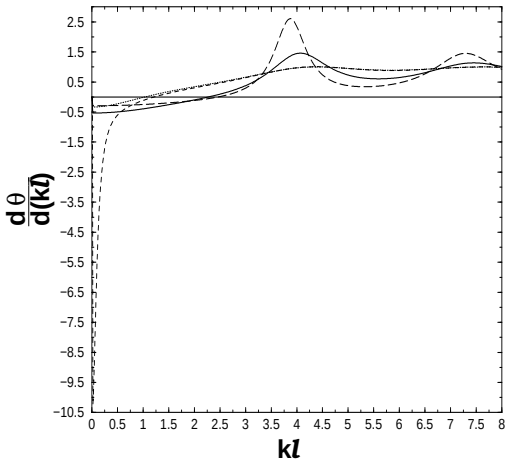

FIG. 6. The system under consideration is shown in Fig.4. The plot is of $d\theta/d(kl)$ versus kl for the system for different values of Vl^2. The dotted curve is for $Vl^2 = -2$, the dashed curve is for $Vl^2 = -2.1$, the solid curve is for $Vl^2 = -5$, the long dashed curve for $Vl^2 = -8$. We use $\hbar = 1, 2m = 1$.

One can prove that

$$\bar{\rho} = \mid a \mid^2 + \mid b \mid^2 = \frac{1 - \mid r^{'} \mid^4}{\mid 1 - r^{'2}\tau^2 \mid^2},$$

for any energy dependent reflection amplitude $r^{'}$ of one of the two identical scatterers in Fig.4, where, $\tau = e^{ikl}$. Hence as indicated by Eq. 11, it would be interesting if we can obtain a good estimate of $\bar{\rho}$ or ρ' from θ. In the appendix I it is explained that if $\frac{dr'}{dE} = \frac{dt'}{dE} \to 0$ (which means the scatterers are non-dispersive and that only happens at high energy in 1D, 2D and 3D) then, $\frac{d\theta}{d(kl)}$ reduces to the expression $\frac{1-|r^{'}|^4}{|1-r^{'2}\tau^2|^2}$, and then therefore, $\frac{d\theta}{d(kl)} = \bar{\rho}$. It is shown in section III of Ref. [18] (see Eq. 6 and 7 therein), that to relate $\frac{d\theta}{dE}$ to the global DOS, one has to neglect the energy dependence of the self energy, that depends on the coupling of the system to the leads, i.e., r' and t'. Thus our results are consistent with that. The exact $\frac{d\theta}{d(kl)}$ is shown in Fig.5 by the solid curve. Note that in the relevant energy regime ($|\frac{E}{V}| > 1$), the solid curve is very close to the dashed and dotted curves, which means FSR works very well for the local DOS as well as for the global DOS. But for $|\frac{E}{V}| < 1$, $\frac{d\theta}{d(kl)}$ deviates from $\bar{\rho}$. But since transport effects in weak localization or diffusive or ballistic regime occur at Fermi energies, that is normally higher in semiconductors as well as metals in comparison to the energy where the two curves deviate substantially from each other, Friedel sum rule is often useful in condensed matter to obtain a good estimate of local DOS as well as global DOS.

$d\theta/dE$ is also well known as Wigner delay time [21,22]. In the stationary phase approximation, it gives the time spent by the scattered particle at the impurity site. In the low energy regime, where dispersion becomes significant, the stationary phase approximation is not valid and $d\theta/dE$ can become negative and does not give a meaningful particle delay time. In this regime $d\theta/dE$ becomes negative as the phase velocity becomes larger than the group velocity and even larger than the velocity of light, and although such super-luminous particles can be detected experimentally they cannot carry any signal or information. In Fig.6 we show the negative behavior of $d\theta/d(kl)$. We find that as the strength of the impurities is varied, $d\theta/d(kl)$ can become more or less negative (see Fig.6), maximizing at $Vl^2 = -2.1$ for the symmetric delta potentials. The energy regime, where $d\theta/d(kl)$ can be negative remains the same for all V and always $|\frac{E}{V}| < 1$. We have checked for all these values of V that apart from this insignificant energy range, FSR works very well. FSR has a close counterpart in quantum mechanics called Levinson's theorem. It is known that Levinson's theorem also breaks down in the presence of zero energy bound states [1] that can be degenerate with scattering states.

III. WIGNER DELAY TIME IN QUASI-ONE-DIMENSIONS

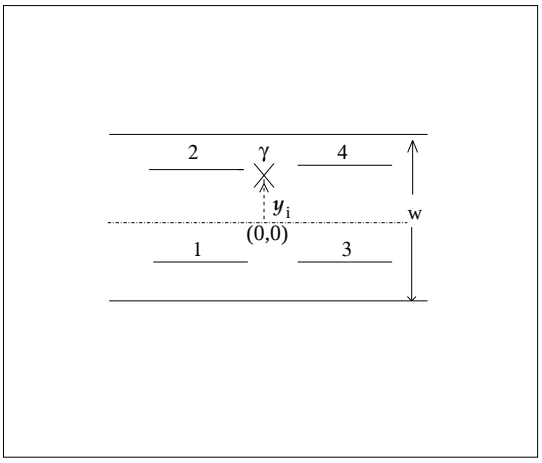

FIG. 7. Here we show a quantum wire of width W. The dash-dotted curve is a line through the middle of the quantum wire, and it is also taken to be the x-axis. The origin of the coordinates is shown in the figure. A delta function potential $V(x,y) = \gamma\delta(x)\delta(y-y_i)$ is situated at $x = 0$ and $y = y_i$ and marked as $\times$. We consider scattering effects when the incident electron is from the left. The sub-bands on the left of the impurity is denoted as 1 for the first mode (i.e., its wave function can be obtained by putting n=1 in Eq.(14) with appropriate sign for k_n) and 2 for the second mode (i.e., its wave function can be obtained by putting n=2 in Eq.(14) with appropriate sign for k_n). Similarly the sub-bands on the right of the impurity is denoted as 3 for the first mode (i.e., its wave function can be obtained by putting n=1 in Eq.(14) with appropriate sign for k_n) and 4 for the second mode (i.e., its wave function can be obtained by putting n=2 in Eq.(14) with appropriate sign for k_n). The impurity at $\times$ mixes these wave functions to give a scattering matrix element t'_{mn} from mode m to mode n.

In Fig.7 we consider a quasi-one-dimensional quantum wire with an attractive impurity at $(0,\ y_i)$, having electrons confined along the y-direction but free to move along the x-direction. While the states far away from the impurity are good momentum states, the impurity can mix the different modes and in this region of mode mixing, the wave function is $\psi(x,y) = \Sigma_n c_n(x)\chi_n(y)$, where $\chi_n(y)$ are the transverse wave functions in the absence of the impurity and $c_n(x)$ are position dependent coefficients that has to be determined by mode matching. The confining potential in the y-direction or the transverse direction is taken to be hard wall. Thus the transverse wave-function is of the form $\chi_n(y) = Sin\frac{n\pi}{W}(y+\frac{W}{2})$. For a given width W of the quantum wire one can choose the energy range of the incident electron such that only two modes are propagating, although, all the other modes (infinite in number, showing that the internal wave function can have infinite degrees of freedom, which makes it difficult to calculate the exact local DOS from the internal wave function) will be present but as evanescent modes. For example, if the energy of the electron be E then for propagation in the n-th transverse mode (in short we will refer this as n-th mode) the wave-function is of the form

$$Sin\frac{n\pi}{W}(y+\frac{W}{2})\ \ e^{ik_n x} \tag{14}$$

where $k_n = \sqrt{E-E_n}$, E_n being $\frac{n^2\pi^2}{W^2}$ and $n = 1,2,3,\cdots\infty$. Here we have used $\hbar = 2m = 1$. To have the n-th mode to be propagating it is necessary that $k_n^2 > 0$ or

$$n < \frac{W}{\pi}\sqrt{E}. \tag{15}$$

Thus we can choose the energy range where there will be two propagating modes, i.e., $n = 1$ and $n = 2$ satisfy condition (15). The rest of the modes ($n > \frac{W}{\pi}\sqrt{E}$) will be evanescent, whose wave functions are of the form

$$Sin\frac{n\pi}{W}(y+\frac{W}{2})\ \ e^{-\kappa_n x}, \tag{16}$$

where $\kappa_n = \sqrt{E_n - E}$. These evanescent modes just renormalize the scattering matrix elements and drop out of the problem. The transmission amplitude from m-th incident mode to n-th scattered mode is given by [9]

$$t'_{mn} = -\frac{i\Gamma_{mn}}{2d\sqrt{k_m k_n}}, \tag{17}$$

$$\text{where} \quad d = 1 + \sum^{e}\frac{\Gamma_{nn}}{2\kappa_n} + i\sum^{p}\frac{\Gamma_{nn}}{2k_n}. \tag{18}$$

Here $\sum^e$ denotes the sum over all evanescent modes and $\sum^p$ denotes the sum over all propagating modes. Eq.(17) holds only for inter-subband transmission amplitudes and all reflection amplitudes. When we say reflection amplitude we mean the following. For an electron incident from the left, all outgoing channels to the left are reflection channels. According to this convention t'_{11}, t'_{22}, t'_{21} and t'_{12} are reflection amplitudes. Inter-subband transmission amplitude are then obviously t'_{14} and t'_{23}. The intra-subband transmission amplitudes t'_{13} and t'_{24} (according to numbering of channels explained in Fig.7) are given by

$$t'_{13} = 1 + t'_{11} \quad \text{and} \quad t'_{24} = 1 + t'_{22}. \tag{19}$$

Here Γ_{nm} is the strength of coupling between the n-th mode and the m-th mode. If we take the impurity to be a delta function potential i.e., $V(x,y) = \gamma\delta(x)\delta(y-y_i)$, and the confining potential in the y-direction to be hard wall ($V = \infty$ for $-\frac{W}{2} \geq y \geq \frac{W}{2}$, and 0 everywhere else except the impurity site $\times$) (see Fig.7) then

$$\Gamma_{nm} = \gamma Sin\frac{n\pi}{W}(y_i+\frac{W}{2})Sin\frac{m\pi}{W}(y_i+\frac{W}{2}).$$

Apart from the two propagating modes we consider two evanescent modes and truncate the infinite series of evanescent modes (note that although the series is strongly converging, the reason for truncating is different, stronger and explained in more detail after Fig. 12) in Eq. (18) and so Eq. (18) becomes

$$1 + \frac{\Gamma_{33}}{2\kappa_3} + \frac{\Gamma_{44}}{2\kappa_4} + i\left(\frac{\Gamma_{11}}{2k_1} + \frac{\Gamma_{22}}{2k_2}\right) = d_2 \ \text{(say)}. \qquad (20)$$

The lowest evanescent mode (putting n=3 in Eq. (16) gives its wave function) has even parity in the transverse direction. For a negative impurity potential *i.e.*, $\gamma < 0$, it also has a bound state at $E = E_{3b}$, where E_{3b} is given by the solution of

$$1 + \frac{\Gamma_{33}}{2\kappa_3} + \frac{\Gamma_{44}}{2\kappa_4} = 0. \qquad (21)$$

Since $E_{3b} < \frac{9\pi^2}{W^2}$, E_{3b} can be degenerate with scattering states (the n=1 and n=2 modes are the scattering states). The higher evanescent mode (putting n=4 in Eq. (16) gives its wave function) has odd parity in the transverse direction and this too has a bound state at $E = E_{4b}$, where E_{4b} is given by the solution of

$$1 + \frac{\Gamma_{44}}{2\kappa_4} = 0. \qquad (22)$$

Once again depending on γ, E_{4b} can be degenerate with the scattering states. The effect of including more evanescent modes is just to renormalize the strength of the impurity potential and does not give anything new [9].

The scattering matrix in this case is

$$S = \begin{bmatrix} t_{11}^{'} & t_{12}^{'} & t_{13}^{'} & t_{14}^{'} \\ t_{21}^{'} & t_{22}^{'} & t_{23}^{'} & t_{24}^{'} \\ t_{31}^{'} & t_{32}^{'} & t_{33}^{'} & t_{34}^{'} \\ t_{41}^{'} & t_{42}^{'} & t_{43}^{'} & t_{44}^{'} \end{bmatrix} = \begin{bmatrix} r_{2c} & t_{2c} \\ \hat{t}_{2c} & \hat{r}_{2c} \end{bmatrix}, \qquad (23)$$

$$\text{where} \quad r_{2c} = \begin{bmatrix} t_{11}^{'} & t_{12}^{'} \\ t_{21}^{'} & t_{22}^{'} \end{bmatrix}$$

$$\text{and} \quad t_{2c} = \begin{bmatrix} t_{13}^{'} & t_{14}^{'} \\ t_{23}^{'} & t_{24}^{'} \end{bmatrix}.$$

$\hat{t}_{2c} = t_{2c}$ due to time reversal symmetry and $\hat{r}_{2c} = r_{2c}$ for a symmetric scatterer as that considered here. Now once again due to micro-reversebility $t_{12}^{'} = t_{21}^{'}$. Also $t_{12}^{'} = t_{14}^{'}$ because in both $t_{12}^{'}$ and $t_{14}^{'}$ the density of states in the input as well as the output channel is the same, and also the incident channel momenta and the outgoing channel momenta are the same in the transverse as well as in the propagating direction. Also $t_{23}^{'} = t_{41}^{'}$ because transmission amplitude should be independent of the position of the observer i.e., whether the observer is looking into the plane of the paper or out of the plane of the paper. Thus among the 16 matrix elements in Eq. (23) we are left with only 5 that are distinct. They are $t_{11}^{'}, t_{12}^{'}, t_{22}^{'}, t_{13}^{'}$ and $t_{24}^{'}$.

From Eq. (17) and (19),

$$t_{11}^{'} = -\frac{i\Gamma_{11}}{2d_2k_1}, \qquad (24)$$

$$t_{12}^{'} = -\frac{i\Gamma_{12}}{2d_2\sqrt{k_1k_2}}, \qquad (25)$$

$$t_{22}^{'} = -\frac{i\Gamma_{22}}{2d_2k_2}, \qquad (26)$$

$$t_{13}^{'} = \frac{1 + \frac{\Gamma_{33}}{2\kappa_3} + \frac{\Gamma_{44}}{2\kappa_4} + i\frac{\Gamma_{22}}{2k_2}}{d_2} \quad \text{and} \qquad (27)$$

$$t_{24}^{'} = \frac{1 + \frac{\Gamma_{33}}{2\kappa_3} + \frac{\Gamma_{44}}{2\kappa_4} + i\frac{\Gamma_{11}}{2k_1}}{d_2} \ . \qquad (28)$$

Knowing these matrix elements, the scattering matrix is completely known and θ can also be calculated.

We find some further relationships between the scattering phase shifts as follows. First of all

$$arg(t_{11}^{'}) = arg(t_{22}^{'}) = tan^{-1}\frac{Re(d)}{Im(d)}. \qquad (29)$$

Secondly, when $\frac{4\pi^2}{W^2} < E_{3b} < \frac{9\pi^2}{W^2}$, i.e., the bound state of the 3rd subband lies in the energy range where one can have two propagating subbands, then the bound state E_{3b} drastically changes the scattering matrix elements in that energy range. So in this energy range $\frac{4\pi^2}{W^2}$ to $\frac{9\pi^2}{W^2}$ we find

$$arg(t_{12}^{'}) \mp \frac{\pi}{2} = \theta + \pi. \qquad (30)$$

Here negative sign is to be taken when E_{3b} lies in this energy range. Otherwise the positive sign has to be taken. θ is to be calculated from Eq. (2) using Eq. (23). Thirdly we find

$$arg(t_{11}^{'}) \pm \pi = arg(t_{12}^{'}). \qquad (31)$$

Note that in contrast to Eq. (30) here the choice of $\pm$ sign is arbitrary. However consistent with this choice is the following

$$arg(t_{11}^{'}) \pm \frac{\pi}{2} = \theta + \pi, \qquad (32)$$

where once again + sign is to be taken when E_{3b} is present in this energy range and - sign is to be taken when absent.

We thus find very simple analytical expressions for θ in the sense that one need not calculate it from a 4×4 scattering matrix but can calculate it from the argument of a single matrix element like $t_{11}^{'}$ or $t_{12}^{'}$ or $t_{22}^{'}$. These relations are analogous to Eq. (4) in section I obtained for purely one dimensional case, i.e., one need not calculate θ from 2×2 matrix but one can find it from the argument of a single matrix element.

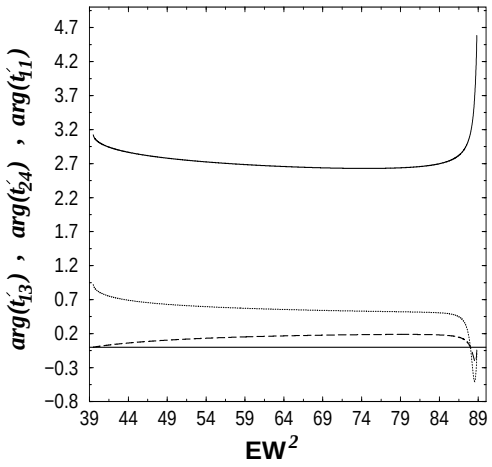

FIG. 8. The system under consideration is shown in Fig. 7. The plot is of the argument of various transmission amplitudes ($arg(t^{'}_{mn})$ in radians) from incident channel m to propagating channel n versus EW^2 . The solid curve gives $arg(t^{'}_{11})$, the long dashed curve gives $arg(t^{'}_{13})$ and the dotted curve gives $arg(t^{'}_{24})$. We use $\gamma = -10$, $y_i = .21W$ and $x_i = 0$

In Fig. 8, we plot only the distinct arguments of the scattering amplitudes versus energy of the incident electron. We find that all of them show negative slopes over a very large range of energy and as already discussed, such negative slopes give rise to fundamental questions in quantum mechanics [21,22]. Now in Q1D we find that this negative slope is not restricted to low energy but can occur at any arbitrary energy. Notice for example, $arg(t'_{13})$ and $arg(t'_{24})$ show larger negative slopes at the highest possible energies for two channel propagation. The rest of this section will be devoted to understanding these negative slopes that at first sight looks very different in nature and character in the three curves in Fig. 8, and also to understanding what will happen when there are more than two propagating modes. We will address the FSR in the next section.

It is to be noted that among all these scattering matrix elements $t^{'}_{11}$ and $t^{'}_{13}$ exist in the single channel regime (i.e., $\pi^2 < EW^2 < 4\pi^2$) where $t^{'}_{11}$ is the reflection amplitude and $t^{'}_{13}$ is the transmission amplitude. The phase of t'_{13} in the single channel regime is known to change discontinuously by π when t'_{13} is 0, i.e., t'_{13} has a zero in real energy. In the two channel regime if we write from simplifying Eq. (27)

$$t^{'}_{13} = \frac{k_2(2\kappa_3 + g_3) + i\kappa_3 g_2}{k_2(2\kappa_3 + g_3) + i\kappa_3(g_2 + \alpha g_1)}, \tag{33}$$

where $\alpha = \frac{k_2}{k_1}$ and $g_s = \frac{2\kappa_4}{\Gamma_{44}+2\kappa_4}\ \Gamma_{ss}$; with s=1,2,3. then interestingly, we see that it has a zero in complex energy and not in real energy.

If we modify the Breit-Wigner line shape formula of 1D to include complex zeroes and write

$$t_{mbw}(E) = A\ \frac{E - E_0 + i\Gamma_0}{E - E_p + i\Gamma_p}\ , \tag{34}$$

where A is a normalization factor, then just as Γ_p gives the scale over which $arg[t_{mbw}(E)]$ increase at $E = E_p$, Γ_0 gives a scale over which $arg[t_{mbw}(E)]$ decrease at $E = E_0$ where $|t_{mbw}(E)|^2$ also shows a minimum at $E = E_0$ (but not zero). One can check this very easily (let us say, when E_0=2, E_p=1 and $\Gamma_0 = \Gamma_p = 0.5$) and so we do not demonstrate it here. Now from Eq. (33) we see that at an energy which satisfies the condition

$$2\kappa_3 + g_3 = 0, \tag{35}$$

the real part of the numerator in Eq. (33) is zero. Condition (35) is the same as the condition (21) for a bound state E_{3b} coming from the 3rd subband that is degenerate with scattering states. So, around this energy where Eq.(35) is satisfied (lets say at $E = E_{3b} \equiv E_0$) $arg(t'_{13})$ will undergo a drop over an energy scale determined by the imaginary part, $\kappa_3 g_2$, i.e., $\Gamma_0 \equiv \kappa_3 g_2$.

It can be seen in Fig.9 that $|t^{'}_{13}|^2$ (dotted curve) shows a narrow minimum around an energy $EW^2 \simeq 84$ (which is the solution of Eq. (35) or Eq. (21)) and at this energy $arg(t^{'}_{13})$ shows a very sharp drop over a narrow energy range determined by $\kappa_3 g_2$. Hence by decreasing/increasing this quantity $\kappa_3 g_2$ we can make the phase drop sharper/broader. g_2 can be made smaller in two ways, first by decreasing γ and second by taking the impurity closer to a node in the transverse wave function. The plot for a decreased value of γ is shown in Fig.10 and it confirms this.

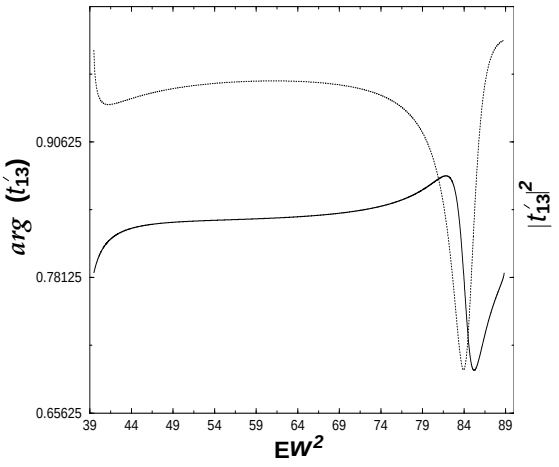

FIG. 9. The system under consideration is shown in Fig.7. The solid curve gives $arg(t^{'}_{13})$ in radians shifted by $\frac{\pi}{4}$ radians in the y-direction and the dotted curve gives $|t^{'}_{13}|^2$. Both the functions are plotted versus EW^2 using $x_i = 0$, $y_i = .45W$ and $\gamma = -15$.

Note that the quantity $\kappa_3 g_2$ is actually energy dependent. But in Fig.9 and Fig.10 $\kappa_3 g_2$ is so small that the drop occurs over a scale in which $\kappa_3 g_2$ is roughly constant. For larger values of $\kappa_3 g_2$, the phase drop will be determined by a complex competition between κ_3 and g_2. This is shown in Fig.11. First of all the scale of the phase drop becomes so large that any sensitivity to the position of the bound state can not be seen. Secondly, $\kappa_3 g_2$ can not be taken to be a constant over this large scale and the enhancement of the negative slope for $EW^2 > 79$ is a signature of the fact that here $\kappa_3 \to 0$ and so $\kappa_3 g_2 \to 0$ as EW^2 increases.

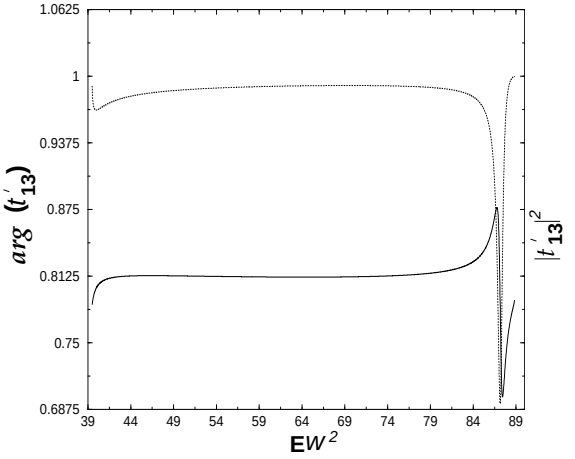

FIG. 10. The system under consideration is shown in Fig.7. The solid curve gives $arg(t_{13}^{'})$ in radians shifted by $\frac{\pi}{4}$ radians in the y-direction and the dotted curve gives $|t_{13}^{'}|^2$. Both the functions are plotted versus EW^2 using $x_i = 0$, $y_i = .45W$ and $\gamma = -10$

Similarly if we rewrite Eq.(28) as

$$t_{24}^{'} = \frac{k_1(2\kappa_3 + g_3) + i\kappa_3 g_1}{k_1(2\kappa_3 + g_3) + i\kappa_3(g_1 + \beta g_2)},$$

where $\beta = \frac{k_1}{k_2}$; then it is clear that the behavior of $arg(t_{24}^{'})$ will be qualitatively the same. It is indeed found in Fig.8 that the behavior of $arg(t_{24}^{'})$ is similar to that of $arg(t_{13}^{'})$.

$\theta = \frac{1}{2i} ln[det[S]]$ is shown in Fig.12 as a function of energy, for different values of γ. The minimum in θ follows the E_{3b} and so the energy range where the slope of θ versus E is negative is determined by the E_{3b}. Note that when E_{3b} goes out of this energy range the θ versus E has a positive slope everywhere. So in Fig.12, the negative slope arises whenever a bound state E_{3b} is degenerate with the scattering states (n=1 and n=2), and nonmonotonously scatter and disperse the scattering states. For weaker impurities in Q1D, the negative slope occur at higher energies and also are steeper as demonstrated in Fig.12. This is in contrast to what happens in 1D and demonstarted in Fig. 6, that the energy where the negative slopes occur is always for $E/V < 1$.

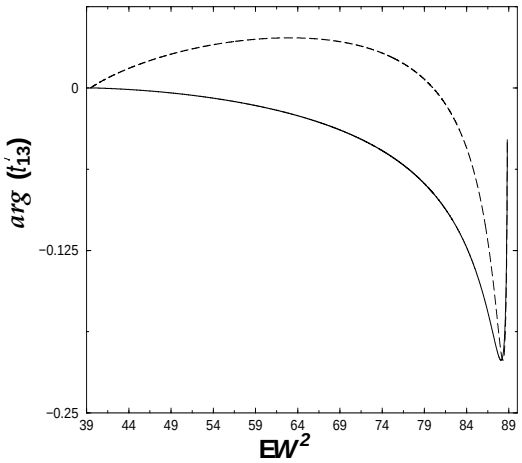

FIG. 11. The system under consideration is shown in Fig.7. The solid curve gives $arg(t_{13}^{'})$ in radians shifted by 2π radians in the negative y-direction versus EW^2 for $\gamma = -47.1371$. The dashed curve is for $\gamma = -25.197$. We use $x_i = 0$ and $y_i = .21W$.

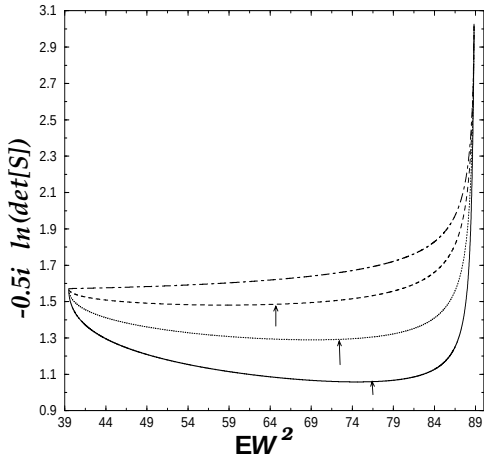

FIG. 12. The system under consideration is shown in Fig.7. The plot is of θ in radians versus EW^2 for different γ. The dot-dashed curve is shifted by π radians in y-direction for $\gamma = -47.1371$, corresponding E_{3b} is at $EW^2 = 35$ which is less than the propagating threshold $EW^2 \simeq 39$ of the second transverse mode. The dashed curve is for $\gamma = -25.197$, corresponding E_{3b} is at $EW^2 = 80$. The dotted curve is for $\gamma = -15$, corresponding E_{3b} is at $EW^2 = 86.606$. The solid curve is for $\gamma = -10$, corresponding E_{3b} is at $EW^2 = 87.982$. We use $y_i = .21W$ and $x_i = 0$. The arrows accentuate the positions of the minima that is shifting towards higher energies for weaker impurities.

We have used two evanescent modes in our calculations because one can include as many evanescent modes without changing the nature of the negative slopes as long as the positions of the bound states E_{3b} and E_{4b} remain the same. One can check this that with four evanescent modes and $\gamma = -6.46584$, the negative slopes are the same as in Fig. 8, which means that the third and the fourth evanescent modes just renormalizes γ from -6.46584 to -10. The exact renormalization takes place according to a formula $\gamma^h = \gamma^n/d$, where γ^h is the γ value used here and γ^n is the renormalized value of γ when we use m evanescent modes instead of two. $d = (1 + \Gamma^n_{55}/(2\kappa_5) + \Gamma^n_{66}/(2\kappa_6)....\Gamma^n_{mm}/(2\kappa_m)$, where $\Gamma^n_{mm} == \gamma^n Sin\frac{m\pi}{W}(y_i + \frac{W}{2})^2$. Solving this one can find the renormalized value of γ i.e., γ^n that keep the minimum of any of the curves for the scattering phase shifts considered here unchanged. It is worthwhile mentioning that at the band edges (i.e., $E \approx 39$ and 89, in the figures considered in this section), the value of any curve is independent of the number of evanescent modes, as all the modes get decoupled there. In other words, number of evanescent modes considered does not change the nature of the negative slopes. Only the positions of the bound states are important.

In order to generalize to arbitrary number of propagating channels we change our notations slightly. For electrons incident from the left/right, we call the scattered channels towards the left/right as reflection channels (the rest being transmission channels) and change our notation to

$$\tilde{r}_{11} = t^{'}_{11} \ , \tag{36}$$

$$\tilde{r}_{22} = t^{'}_{22} \ , \tag{37}$$

$$\tilde{r}_{12} = t^{'}_{12}. \tag{38}$$

Thus all possible reflection channels are distinct. All the intra-subband transmission channels are also distinct and they are denoted as $\tilde{t}_{11}$ and $\tilde{t}_{22}$ where

$$\tilde{t}_{11} = t^{'}_{13} \tag{39}$$

$$\text{and} \quad \tilde{t}_{22} = t^{'}_{24}. \tag{40}$$

All other scattering matrix elements are equal to one of these 5 elements. In this notation the only difference is that the lowest channel (n=1) on the transmission side is marked 1 instead of 3. So when we say $\tilde{t}_{11}$ we mean transmission amplitude from the n=1 channel on the left to the n=1 channel on the right. We find from Eqs. (29), (30), (31) and (32)

$$\frac{d}{dE}\, arg(\tilde{r}_{mn}) = \frac{d}{dE}\,(\frac{1}{2i} ln[det[S]]) \tag{41}$$

We find the above relation to be true for any number of propagating modes. So m and n can take any integer value less than or equal to p, where p is the total number of propagating modes. For two propagating modes p=2, for three propagating modes p=3 and so on. So Eq.(41) is analogous to the 1D case given in Eq.(4). That is when the dimension of the matrix S becomes very large, then it is sufficient to consider the argument of a single matrix element in order to calculate the complicated quantity on the RHS of Eq. 41. In the energy regime where there are two propagating channels, the negative slopes in θ versus incident energy curves are determined by E_{3b}, and when there are 3 propagating channels then the negative slopes are determined by E_{4b} and so on.

The scattering phase shifts of transmission channels i.e. $arg(\tilde{t}_{mn})$, where again m and n can take all possible integer values less than or equal to p, show sharp or gentle phase drops when the scattering states are degenerate with a bound state, depending on the value of the imaginary part in the numerator of $\tilde{t}_{mn}$. In the single channel regime the imaginary part in the numerator is zero and phase drops take the limiting value when the phase drops are absolutely discontinuous by π. Just as the discontinuous phase drop in single channel case do not affect θ in any way, the phase drops of the $arg(\tilde{t}_{mn})$ also do not affect θ in any way and θ behaves similarly as $arg(\tilde{r}_{mn})$.

IV. DENSITY OF STATES AND FRIEDEL SUM RULE IN QUASI-ONE-DIMENSION

The local DOS is given by the following expression [9]

$$\rho_R = \int_R dx \int_{\frac{-W}{2}}^{\frac{W}{2}} dy \sum_{m,k_m} \delta(E - E_{m,k_m}) \mid \psi_{m,k_m}(x,y) \mid^2 \tag{42}$$

Here E is the incident energy and R is the integration region where modes are mixed. m and k_m are the two quantum numbers that define an incident electron wavefunction, $A_m e^{ik_m x} Sin\frac{m\pi}{W}(y + \frac{W}{2})$ whose energy is E_{m,k_m}, where we have taken that the electron is incident from the left i.e., $x < 0$. $\psi_{m,k_m}(x,y)$ is the wavefunction in the region of mode mixing and $\psi_{m,k_m}(x,y) = \sum_n c^{(m)}_n(x,k_n) Sin\frac{n\pi}{W}(y + \frac{W}{2})$. Here $c^{(m)}_n(x,k_n) = C_n e^{ik_n x}$ for $n = 1$ and $n = 2$ and $c^{(m)}_n(x,k_n) = C_n e^{-\kappa_n x}$ for $n > 2$; x being greater than or equal to 0. The coefficients C_n can be determined by using the mode matching technique. The mode matching has been done in details by Bagwell [9]. Here the delta function potential is taken to be extending from $-\epsilon$ to $+\epsilon$ which has to be set to be tending to 0 in the end. ρ_{0R} can be determined by replacing $\psi_{n,k_n}(x,y)$ by the plane wave states in absence of the scatterer and doing the integration again.

Thus we find that for any non-zero incident energy

$$(\rho - \rho_0)_R = \frac{2}{hv_1}[|t_{13}|^2 + |t_{14}|^2 + |t_{15}|^2 + \cdots]$$

$$+\frac{2}{hv_2}[|t_{23}|^2+|t_{24}|^2+|t_{25}|^2+\cdots]. \quad (43)$$

Here $v_1=\frac{\hbar k_1}{m}, v_2=\frac{\hbar k_2}{m}$ and $t_{mn}=\frac{C_n}{A_m}$. t_{mn} can be obtained by solving the matrix Eqs. given in Ref. [9] (see Eq. 23 therein and we have used the same notation i.e., t_{mn} here is the same as t_{mn} in Eq. (23) of Ref. [9]). As can be seen in Fig.12 that $\frac{d\theta}{dE}$ is negative over a very large energy range while $(\rho-\rho_0)_R$ as given by Eq.43 is positive.

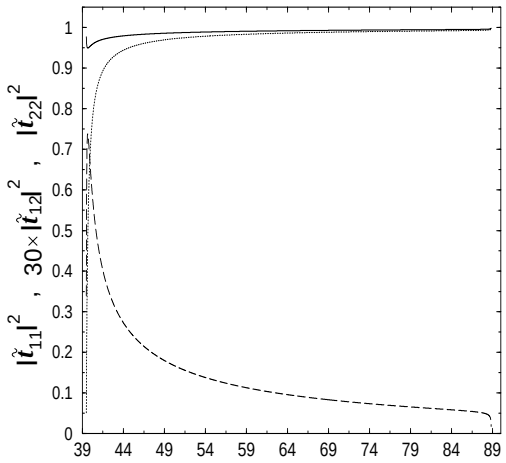

FIG. 13. The system under consideration is shown in Fig.7 with $\gamma=1$. The Fig. shows some important scattering probabilities. The solid curve gives $|\tilde{t}_{11}|^2$ and it shows that for $EW^2>50$, a particle incident in the first propagating mode does not feel the scatterer at all, and is almost entirely transmitted intra-channel, $|\tilde{t}_{11}|^2$ being close to unity. The dotted curve gives $|\tilde{t}_{22}|^2$ and once again for $EW^2>50$, it is close to unity signifying that a particle incident in the second propagating channel is almost entirely transmitted intra-channel. So $EW^2>50$ is the WKB regime where the potential scatters the incident electron very weakly. The dashed curve gives 30 times $|\tilde{t}_{12}|^2$ and shows strong energy dependence not only for $EW^2<50$ but also around the highest energy ($EW^2\approx 89$) or in the extreme WKB limit, its absolute value being extremely small there signifying extremely low inter-channel transmission i.e., the incoming particle does not feel the scatterer.

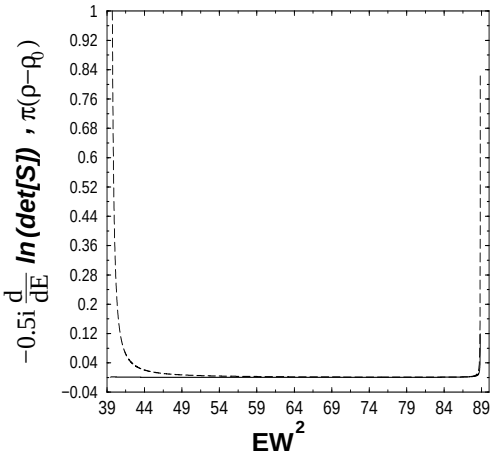

FIG. 14. The system under consideration is shown in Fig.7 with $\gamma=1$. The solid curve gives $\pi(\rho(E)-\rho_0(E))$ and the dashed curve gives -0.5$i\frac{d}{dE}ln(det[S])$. The two curves deviate from each other, where ever the curves in Fig. 13 are strongly energy dependent. Otherwise they agree.

Note that if we calculate the global DOS by taking the integration region to be from $-\infty$ to ∞ instead of just the region R where the modes are mixed then Eq. 43 remain the same. One will get some extra integrals that are indefinite integrals but using the current conservation condition it can be analytically proved (see appendix II) that they cancel each other. This means the contribution to $\rho(E)$ and that to $\rho_0(E)$ coming from outside the region R cancel each other in the absence of a term like ρ_q/l as in section II. Thus in this case (the proof is given in appendix II)

$$\rho(E)-\rho_0(E)=(\rho-\rho_0)_R$$

and both of them deviate identically from $\frac{1}{\pi}\frac{d\theta}{dE}$ due to strong dispersion, at any arbitrary energy.

Since the negative slopes are due to the bound states supported by the negative delta function potential, one may ask what happens for a positive delta function potential that does not support any bound state. This situation is discussed below and it also elaborates the uniqueness of the Q1D, with respect to the violation of Friedel sum rule and shows that large violation can occur in the extreme WKB limit. Fig 13 shows the energy dependence of some important scattering probabilities. As in 1D the scattering probabilities are strongly energy dependent for $EW^2<50$. For $EW^2>50$ all the curves vary slowly with energy (non-dispersive scattering). However, one scattering probability $|\tilde{t}_{12}|^2$ is also very strongly energy dependent at the highest energy of $EW^2\approx 89$. ($k_m^2/V>>1$). In this regime scattering is almost entirely intra-channel as can be seen that $|\tilde{t}_{11}|^2$ and $|\tilde{t}_{22}|^2$ are both almost unity. All other scattering probabilities like reflection probabilities and inter-channel scattering probabilities like $|\tilde{t}_{12}|^2$ are extremely small. There are several

other scattering matrix elements that are identical to $\tilde{t}_{12}$. Although being small, they can have strong energy dependence, or their energy derivative can be very large. As can be seen in Fig. 13 that the dashed curve bends down with a steep slope at $EW^2 \approx 89$. It is found in Fig. 14 that there is a strong violation of Friedel sum rule in the non-WKB regime as in 1D and also in the extreme WKB regime ($EW^2 \approx 89$ where $k^2/V >> 1$ and scattering is almost completely intra-channel) quite unlike that in 1D. It can be seen in Fig. 13 that in the mid-energy range, the scattering probabilities are not very energy dependent and the Friedel sum rule holds in this mid-energy range as can be seen in Fig. 14. But at regimes where the scattering leads to strong dispersion, FSR is violated. As the strength of the positive delta function potential is increased, this regime where the scattering probabilities are not strongly energy dependent becomes narrower and Friedel sum rule is violated at all energies.

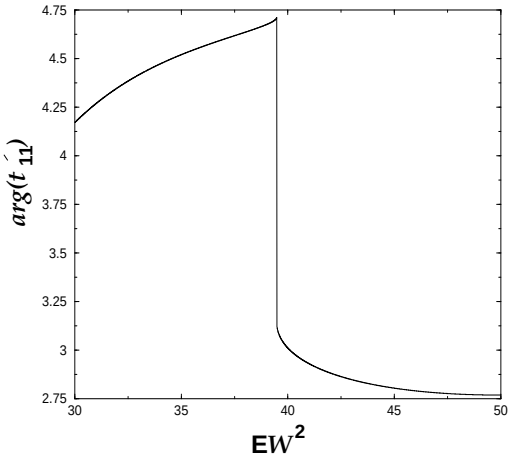

FIG. 15. The system under consideration is shown in the Fig.7. The plot is of $arg(t_{11}^{'})$ in radians versus EW^2. This plot is for $\gamma = -25.197$, $x_i = 0$ and $y_i = .45W$.

V. PHASE BEHAVIOR AT CRITICAL ENERGIES

Very interesting phase behaviors can be seen at energies where the S-matrix changes dimension. For example for $E \leq \frac{4\pi^2}{W^2}$ there is only one propagating mode and the S-matrix is 2×2. But for $E > \frac{4\pi^2}{W^2}$, there are two propagating modes and the S-matrix is 4×4. The matrix element $t_{11}^{'}$ exists on either side of the energy $\frac{4\pi^2}{W^2}$ and in Fig.15 we show the behavior of $arg(t_{11}^{'})$ in the energy range that includes $EW^2 = 4\pi^2$. Note that it exhibits a discontinuous phase drop by $\frac{\pi}{2}$ at $EW^2 = 4\pi^2$. So far only discontinuous phase drops of π has been observed but never $\frac{\pi}{2}$. From the properties of a 2×2 S-matrix it follows that if there is a discontinuous phase change then it can only be of π [16,17]. So had the S-matrix been 2×2 on either side of $EW^2 = 4\pi^2$ the phase drop would have been π. But since the S-matrix is 2×2 only on one side, including $EW^2 = 4\pi^2$, i.e., $E \leq \frac{4\pi^2}{W^2}$, the phase drop is also one half of π. $|t_{11}^{'}|^2$ also has a zero at $EW^2 = 4\pi^2$ for all possible choice of parameters [9], and this zero is associated with a $\frac{\pi}{2}$ phase jump instead of a π phase jump.

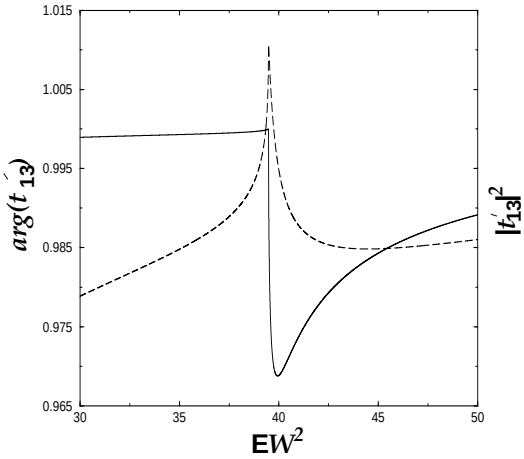

FIG. 16. The system under consideration is shown in the Fig.7. The solid curve gives $|t_{13}^{'}|^2$. The dashed curve is after subtracting 5.27183 radians from $arg(t_{13}^{'})$ in radians. We use $\gamma = +25.197$, $x_i = 0$ and $y_i = .45W$.

Next we take a repulsive δ function potential. It is known [9] that at critical energies like $EW^2 = 4\pi^2$, $|t_{13}^{'}|^2$ shows discontinuities. Here $|t_{13}^{'}|^2$ does not have a zero but exhibits a discontinuous jump. At these points $arg(t_{13}^{'})$ also shows non-analytic behavior as demonstrated in Fig.16. In this case $\frac{d}{dE} arg(t_{13}^{'})$ is discontinuous.

VI. CONCLUSIONS

In a multichannel quantum wire with attractive impurities, negative slopes in the scattering phase shift versus incident energy curves can occur at all possible energies. For weaker defects it happens at higher energies

and the negative slopes are more pronounced. Such negative slopes mean super luminescence [21,22] that can be observed experimentally. Although such a super luminescent particle will not give any information about the particle delay or information delay, they are of interest because they demonstrate fundamental principles in quantum mechanics. Hence Eq. (41) derived in this paper may be of use to experimentalists and theoreticians. Calculations of variation of DOS due to the presence of the scatterer show that FSR can be violated at any arbitrary energy. That is violation of FSR is not restricted to non-WKB regime (the regime where anyway transport does not occur) as in 1D, 2D or 3D. Rather the violation is related to strong energy dependence of the scattering matrix elements (dispersive behavior). While in 1D, 2D and 3D the strong energy dependence of scattering occur only in the non-WKB regime, in Q1D there is no systematics. A Q1D system in the extreme WKB limit can also exhibit strongly energy dependent scattering and there is no definable regime where the FSR will work and hence it may not work even in regimes where transport occurs. For attractive impurities, weaker the impurity, stronger the violation of FSR while for repulsive impurities, stronger the impurity, stronger the violation of FSR. We also show that the discontinuous phase drops in the single channel case have a counterpart in the multichannel case wherein the drops can be continuous and we propose a line shape formula for them in Eq. 34. When there is a third channel of escape for the electron, apart from the channel along which it is incident and the channel where its scattering phase shift is measured, the phase drop becomes continuous. However, these phase drops do not affect $\frac{1}{2i}lnDet[S]$ and hence Friedel sum rule. Finally, we discuss some novel scattering phase shifts at energies where the S matrix changes dimension.

VII. ACKNOWLEDGMENTS

We thank Dr. A. M. Jayannavar for useful discussions.

VIII. APPENDIX I

Considering the symmetric scattering potential in Fig.4, the scattering matrix S of the structure can be found by cascading the scattering matrices of different parts, i.e.,

$$S = \begin{pmatrix} r & t \\ t & r \end{pmatrix} = S_1 \otimes S_2 \otimes S_3,$$

$$\text{where} \quad S_1 = S_3 = \begin{pmatrix} r' & t' \\ t' & r' \end{pmatrix}$$

$$\text{and} \quad S_2 = \begin{pmatrix} 0 & \tau \\ \tau & 0 \end{pmatrix} .$$

Here $\tau = e^{i\phi}$, $\phi = kl$ and $k = \sqrt{\frac{2m}{\hbar^2}E}$. S_2 is the scattering matrix for the free region II of length l between the two scatterers. r' & t' are the reflection & transmission amplitudes due to one of the two potentials when isolated.

After cascading these three matrices the resultant scattering matrix of our system becomes

$$S = \begin{pmatrix} r' + \dfrac{t'^2\tau^2 r'}{1 - r'^2\tau^2} & \dfrac{t'^2\tau}{1 - r'^2\tau^2} \\ \dfrac{t'^2\tau}{1 - r'^2\tau^2} & r' + \dfrac{t'^2\tau^2 r'}{1 - r'^2\tau^2} \end{pmatrix} .$$

And so,

$$det[S] = \left(r' + \frac{t'^2\tau^2 r'}{1 - r'^2\tau^2} \right)^2 - \left(\frac{t'^2\tau}{1 - r'^2\tau^2} \right)^2 \qquad \text{(i)}$$

$$= \frac{1}{(1 - r'^2\tau^2)^2} \, (M + N) \, , \qquad \text{(ii)}$$

$$\text{where} \qquad M = r'^2(1 - r'^2\tau^2)^2 \qquad \text{(iii)}$$

$$\text{and} \qquad N = (1 - r'^2\tau^2) \, (2t'^2 r'^2\tau^2 - t'^4\tau^2). \qquad \text{(iv)}$$

From (i),

$$\frac{\partial det[S]}{\partial \phi} = 2 \left(A \frac{\partial A}{\partial \phi} - B \frac{\partial B}{\partial \phi} \right), \qquad \text{(v)}$$

$$\text{where} \qquad A = r' + \frac{t'^2\tau^2 r'}{1 - r'^2\tau^2} \qquad \text{(vi)}$$

$$\text{and} \qquad B = \frac{t'^2\tau}{1 - r'^2\tau^2} \quad . \qquad \text{(vii)}$$

Using (v), (vi) and (vii) we find

$$\frac{\partial det[S]}{\partial \phi} =$$

$$2 \left[A \left(2r'B + \frac{2r'^3\tau^2 B}{1 - r'^2\tau^2} \right) - B \left(\frac{t'^2 + r'^2 t'^2 \tau^2}{(1 - r'^2\tau^2)^2} \right) \right] \frac{\partial \tau}{\partial \phi}$$

$$+2 \left[A \left(1 + B\tau + \frac{2r'^2\tau^3 B}{1 - r'^2\tau^2} \right) - B \left(\frac{2r'\tau^2 B}{1 - r'^2\tau^2} \right) \right] \frac{\partial r'}{\partial \phi}$$

$$+2 \left[2r'\tau AB - B \left(\frac{2\tau t'}{1 - r'^2\tau^2} \right) \right] \frac{\partial t'}{\partial \phi}. \qquad \text{(viii)}$$

We will neglect the last two terms in comparison to the 1st term in Eq.(viii) but we will retain the energy dependence of r' and t' and the 1st term in Eq.(viii) is actually varying with energy very strongly. Hence our results correspond to real potentials and we do not parameterize the S matrix in a special way. We apply this result to the case of double delta function potential in Fig.5 and illustrate the significance of the last two terms in comparison with the 1st one. We stress that this calculation in this appendix holds even if the δ-function potential is replaced by the square-well or any arbitrary potential. Thus in the regime where $\frac{\partial r'}{\partial \phi} \to 0$ and $\frac{\partial t'}{\partial \phi} \to 0$ and using $\frac{\partial \tau}{\partial \phi} = i\tau$,

$$\frac{\partial det[S]}{\partial \phi}$$

$$= 2\left[A\left(2r'B + \frac{2r'^3\tau^2 B}{1-r'^2\tau^2}\right) - B\left(\frac{t'^2 + r'^2t'^2\tau^2}{(1-r'^2\tau^2)^2}\right)\right] i\tau \ .$$

At this point we substitute the values of A and B from (vi) and (vii) to get

$$\frac{\partial det[S]}{\partial \phi} = 2i \ \frac{1}{(1-r'^2\tau^2)^3} \ N \ . \qquad \text{(ix)}$$

$$\text{Now,} \quad \theta = \frac{1}{2i} ln(det[S]) \qquad \text{(x)}$$

$$\text{and so} \quad \frac{\partial \theta}{\partial E} = \frac{\partial \theta}{\partial \phi} \ \frac{\partial \phi}{\partial E}.$$

From (x), (ii) and (ix)

$$\frac{\partial \theta}{\partial \phi} = \frac{1}{2i} \ \frac{1}{det[S]} \ \frac{\partial det[S]}{\partial \phi}$$

$$= \frac{1}{1-r'^2\tau^2} \ \frac{1}{\frac{M}{N}+1} \ .$$

Multiplying the numerator and denominator by $\frac{(1-r'^2\tau^2)^*}{1-|r'|^4}$, we get

$$\frac{\partial \theta}{\partial \phi} = \frac{1-\mid r' \mid^4}{\mid 1-r'^2\tau^2 \mid^2} \ \frac{(1-r'^2\tau^2)^*}{1-\mid r' \mid^4} \ \frac{1}{\frac{M}{N}+1}$$

$$= \frac{1-\mid r' \mid^4}{\mid 1-r'^2\tau^2 \mid^2} \ Q \ , \qquad \text{(xi)}$$

$$\text{where,} \quad Q = \frac{(1-r'^2\tau^2)^*}{1-\mid r' \mid^4} \ \frac{1}{\frac{M}{N}+1} \qquad \text{(xii)}$$

$$= \left[\frac{(1-r'^{*2}\tau^{*2}) - 1 + \mid r' \mid^4 \mid \tau \mid^4}{1-\mid r' \mid^4} + 1\right] \ \frac{1}{\frac{M}{N}+1} \ ,$$

as $|\tau|^4 = 1$.

As $1 - |r'|^2 = |t'|^2$

$$Q = \left[\frac{-r'^{*2}\tau^{*2} + \mid r' \mid^4 \mid \tau \mid^4}{(1+\mid r' \mid^2)|t'|^2} + 1\right] \ \frac{1}{\frac{M}{N}+1} \ .$$

Now substituting the values of M and N from (iii) and (iv)

$$Q = \frac{\frac{-r'^{*2}\tau^{*2}(1-r'^2\tau^2) + |t'|^2(1+|r'|^2)}{|t'|^2(1+|r'|^2)}}{\frac{r'^2(1-r'^2\tau^2) - t'^2\tau^2(t'^2-2r'^2)}{-t'^2\tau^2(t'^2-2r'^2)}} \ .$$

Using, $r' = \mid r' \mid e^{i\theta_r}$ and $t' = \mid t' \mid e^{i\theta_t}$,

$$Q = [|r'|^2|t'|^2|\tau|^4 e^{2i\theta_t} e^{2i(\theta_t - \theta_r)} - |r'|^4|t'|^2|\tau|^4\tau^2 e^{4i\theta_t}$$

$$-|t'|^4\tau^2 e^{4i\theta_t} - |t'|^4|r'|^2\tau^2 e^{4i\theta_t}$$

$$-2|r'|^4|\tau|^4 e^{2i\theta_t} + 2|r'|^6|\tau|^4\tau^2 e^{2i(\theta_t+\theta_r)}$$

$$+2|r'|^2|t'|^2\tau^2 e^{2i(\theta_t+\theta_r)} + 2|r'|^4||t'|^2\tau^2 e^{2i(\theta_t+\theta_r)}]/D,$$

$$\text{where,} \quad D = (1+\mid r' \mid^2)(-\mid t' \mid^4 \tau^2 e^{4i\theta_t} - \mid r' \mid^4 \tau^2 e^{4i\theta_r}$$

$$+2 \mid t' \mid^2 \mid r' \mid^2 \tau^2 e^{2i(\theta_r+\theta_t)} + \mid r' \mid^2 e^{2i\theta_r}). \qquad \text{(xiii)}$$

Now it follows from unitarity that $e^{2i(\theta_t - \theta_r)} = e^{i\pi} = -1$ and $|\tau|^4 = 1$ and so

$$Q = [-|r'|^2|t'|^2 e^{2i\theta_t} - |r'|^4|t'|^2\tau^2 e^{4i\theta_t} - |t'|^4\tau^2 e^{4i\theta_t}$$

$$-|t'|^4|r'|^2\tau^2 e^{4i\theta_t} - 2|r'|^4 e^{2i\theta_t} + 2|r'|^6\tau^2 e^{2i(\theta_t+\theta_r)}$$

$$+2|r'|^2|t'|^2\tau^2 e^{2i(\theta_t+\theta_r)} + 2|r'|^4|t'|^2\tau^2 e^{2i(\theta_t+\theta_r)}]/D$$

$$= [-e^{2i\theta_t}|r'|^2\{|t'|^2 + 2|r'|^2\} - (|t'|^2 + |r'|^2\{|r'|^2 + |t'|^2\})$$

$$(e^{4i\theta_t}|t'|^2\tau^2 - e^{2i(\theta_t+\theta_r)}2|r'|^2\tau^2)]/D \ .$$

Now inside the {} brackets if we use the fact that $\mid r' \mid^2 + \mid t' \mid^2 = 1$, then

$$Q = [-e^{2i\theta_t}|r'|^2(1+|r'|^2) - e^{4i\theta_t}|t'|^2\tau^2 + 2e^{2i(\theta_t+\theta_r)}|r'|^2\tau^2]/D.$$

Multiplying numerator and denominator above by $e^{-2i(\theta_r+\theta_t)}$ and putting $e^{2i(\theta_t-\theta_r)} = e^{i\pi} = -1$, we get

$$Q = \frac{-e^{-2i\theta_r}|r'|^2(1+|r'|^2) + \tau^2(|t'|^2+|r'|^2) + |r'|^2\tau^2}{D'},$$

$$\text{where, } D' = De^{-2i(\theta_r+\theta_t)}. \qquad \text{(xiv)}$$

Again using $|r'|^2 + |t'|^2 = 1$,

$$Q = \frac{(1+|r'|^2)(\tau^2 - |r'|^2e^{-2i\theta_r})}{D'}. \qquad \text{(xv)}$$

Now from (xiv) and (xiii)

$$D' = (1+|r'|^2)[|r'|^2e^{-2i\theta_t} - |r'|^4\tau^2e^{-2i(\theta_t-\theta_r)}$$

$$-|t'|^4\tau^2e^{2i(\theta_t-\theta_r)} + 2|t'|^2|r'|^2\tau^2].$$

As $\theta_t - \theta_r = \frac{\pi}{2}$,

$$D' = (1+|r'|^2)[|r'|^2e^{-2i\theta_t} + \tau^2(|r'|^2+|t'|^2)^2]$$

where of course $|\ r'\ |^2 + |\ t'\ |^2 = 1$. Substituting D' in Eq.(xv),

$$Q = \frac{\tau^2 - |\ r'\ |^2\ e^{-2i\theta_r}}{\tau^2 + |\ r'\ |^2\ e^{-2i\theta_t}}.$$

Multiplying numerator and denominator of Q by $e^{2i\theta_t}$ and using $e^{2i(\theta_t-\theta_r)} = e^{i\pi} = -1$, we get from (xi)

$$\frac{\partial\theta}{\partial\phi} = \frac{1 - |\ r'\ |^4}{|\ 1 - r'^2\tau^2\ |^2}$$

IX. APPENDIX II

The global density of states is given by

$$\rho(E) = \int_{-\infty}^{\infty} dx \int_{\frac{-W}{2}}^{\frac{W}{2}} dy \sum_{m,k_m} |\psi_{m,k_m}(x,y)|^2\, \delta(E - E_{m,k_m}) \qquad \text{(i)}$$

where $\psi_{m,k_m}(x,y) = \sum_n c_n^{(m)}(x)\chi_n(y)$ and E_{m,k_m} is the energy of an electron in the leads.

$E_{m,k_m} = \frac{m^2\pi^2\hbar^2}{2m_eW^2} + \frac{\hbar^2k_m^2}{2m_e}$, where $m = \pm1, \pm2$, as there are two propagating modes in the leads.

As $\chi_n(y)$'s form an orthonormal set,

$$\rho(E) = \sum_{m,k_m} \delta(E - E_{m,k_m}) \int_{-\infty}^{\infty} dx \sum_n \left|c_n^{(m)}(x)\right|^2$$

$$\rho(E) = \frac{2}{hv_1}\int_{-\infty}^{\infty} dx \sum_n \left|c_n^{(1)}(x)\right|^2 + \frac{2}{hv_2}\int_{-\infty}^{\infty} dx \sum_n \left|c_n^{(2)}(x)\right|^2 \qquad \text{(ii)}$$

Here, $v_1 = \frac{\hbar k_1}{m_e}$ and $v_2 = \frac{\hbar k_2}{m_e}$.

Now,

$$\begin{aligned}\int_{-\infty}^{\infty} dx \sum_n \left|c_n^{(1)}(x)\right|^2 &= \int_{-\infty}^{\infty} \left|c_1^{(1)}(x)\right|^2 dx \\ &+ \int_{-\infty}^{\infty} \left|c_2^{(1)}(x)\right|^2 dx \\ &+ \int_{-\infty}^{\infty} \left|c_3^{(1)}(x)\right|^2 dx + \cdots \\ &= T1(\text{say}),\end{aligned}$$

where electron is incident in the fundamental mode,

$$\begin{aligned}c_1^{(1)}(x) &= e^{ik_1x} + \tilde{r}_{11}e^{-ik_1x} \ \text{ for } \ x < 0 \\ &= \tilde{t}_{11}\ e^{ik_1x} \ \text{ for } \ x > 0 \\ c_2^{(1)}(x) &= \tilde{r}_{12}\ e^{-ik_2x} \ \text{ for } \ x < 0 \\ &= \tilde{t}_{12}\ e^{ik_2x} \ \text{ for } \ x > 0\end{aligned}$$

and for $n > 2$,

$$\begin{aligned}c_n^{(1)}(x) &= t_{1n}\ e^{\kappa_nx} \ \text{ for } \ x < 0 \\ &= t_{1n}\ e^{-\kappa_nx} \ \text{ for } \ x > 0\end{aligned}$$

$$\begin{aligned}T1 = &\int_{-\infty}^{0} dx\left[1 + |\tilde{r}_{11}|^2 + 2|\tilde{r}_{11}|\ Cos(2k_1x + \eta_1)\right] \\ &+ \int_0^{\infty} dx|\tilde{t}_{11}|^2 + \int_{-\infty}^{0} dx|\tilde{r}_{12}|^2 + \int_0^{\infty} dx|\tilde{t}_{12}|^2 \\ &+ |t_{13}|^2 + |t_{14}|^2 + \cdots\cdots\end{aligned}$$

Here, η_1 is defined as $\tilde{r}_{11} = |\tilde{r}_{11}|e^{-i\eta_1}$

Similarly, for electron incident in the first excited mode,

$$\begin{aligned}T2 = &\int_{-\infty}^{\infty} dx \sum_n \left|c_n^{(2)}(x)\right|^2 \\ = &\int_{-\infty}^{0} dx\left[1 + |\tilde{r}_{22}|^2 + 2|\tilde{r}_{22}|\ Cos(2k_2x + \eta_2)\right] \\ &+ \int_0^{\infty} dx|\tilde{t}_{22}|^2 + \int_{-\infty}^{0} dx|\tilde{r}_{21}|^2 + \int_0^{\infty} dx|\tilde{t}_{21}|^2 \\ &+ |t_{23}|^2 + |t_{24}|^2 + \cdots\cdots,\end{aligned}$$

Here, η_2 is defined as $\tilde{r}_{22} = |\tilde{r}_{22}|e^{-i\eta_2}$

Therefore,

$$\rho(E) = 2\left[\frac{1+|\tilde{r}_{11}|^2}{hv_1}\int_{-\infty}^{0} dx \;+\; \frac{1+|\tilde{r}_{22}|^2}{hv_2}\int_{-\infty}^{0} dx + \frac{|\tilde{r}_{12}|^2}{hv_1}\int_{-\infty}^{0} dx + \frac{|\tilde{r}_{21}|^2}{hv_2}\int_{-\infty}^{0} dx + \frac{2|\tilde{r}_{11}|}{hv_1}\int_{-\infty}^{0} dx\ \ Cos(2k_1x+\eta_1) + \frac{2|\tilde{r}_{22}|}{hv_2}\int_{-\infty}^{0} dx\ \ Cos(2k_2x+\eta_2) + \frac{|\tilde{t}_{11}|^2+|\tilde{t}_{12}|^2}{hv_1}\int_{0}^{\infty} dx + \frac{|\tilde{t}_{22}|^2+|\tilde{t}_{21}|^2}{hv_2}\int_{0}^{\infty} dx + \frac{1}{hv_1}\left(|t_{13}|^2+|t_{14}|^2+\cdots\right) + \frac{1}{hv_2}\left(|t_{23}|^2+|t_{24}|^2+\cdots\right)\right]$$

Due to time reversal symmetry, $\tilde{r}_{12} = \tilde{r}_{21}$ & $\tilde{t}_{12} = \tilde{t}_{21}$.
Inside the square bracket [ ],
in the 3rd term we put $\tilde{r}_{12} = \tilde{r}_{21}$,
in the 4th term we put $\tilde{r}_{21} = \tilde{r}_{12}$,
in the 7th term we put $\tilde{t}_{12} = \tilde{t}_{21}$,
in the 8th term we put $\tilde{t}_{21} = \tilde{t}_{12}$.

Therefore,

$$\rho(E) = 2\left[\frac{1+|\tilde{r}_{11}|^2+|\tilde{r}_{21}|^2}{hv_1}\int_{-\infty}^{0} dx + \frac{1+|\tilde{r}_{12}|^2+|\tilde{r}_{22}|^2}{hv_2}\int_{-\infty}^{0} dx + \frac{|\tilde{t}_{11}|^2+|\tilde{t}_{21}|^2}{hv_1}\int_{0}^{\infty} dx + \frac{|\tilde{t}_{12}|^2+|\tilde{t}_{22}|^2}{hv_2}\int_{0}^{\infty} dx + \frac{2|\tilde{r}_{11}|}{hv_1}\int_{-\infty}^{0} dx\ \ Cos(2k_1x+\eta_1) + \frac{2|\tilde{r}_{22}|}{hv_2}\int_{-\infty}^{0} dx\ \ Cos(2k_2x+\eta_2) + \frac{1}{hv_1}\left(|t_{13}|^2+|t_{14}|^2+\cdots\right) + \frac{1}{hv_2}\left(|t_{23}|^2+|t_{24}|^2+\cdots\right)\right]$$

Now adding and subtracting the following terms inside [ ],

$$\frac{|\tilde{t}_{11}|^2}{hv_1}\int_{-\infty}^{0} dx,\ \frac{|\tilde{t}_{21}|^2}{hv_1}\int_{-\infty}^{0} dx,\ \frac{|\tilde{t}_{22}|^2}{hv_2}\int_{-\infty}^{0} dx,\ \frac{|\tilde{t}_{12}|^2}{hv_2}\int_{-\infty}^{0} dx,$$

we get,

$$\rho(E) = 2\left[\frac{1+|\tilde{r}_{11}|^2+|\tilde{r}_{21}|^2+|\tilde{t}_{11}|^2+|\tilde{t}_{21}|^2}{hv_1}\int_{-\infty}^{0} dx + \frac{1+|\tilde{r}_{12}|^2+|\tilde{r}_{22}|^2+|\tilde{t}_{12}|^2+|\tilde{t}_{21}|^2}{hv_2}\int_{-\infty}^{0} dx + \frac{2|\tilde{r}_{11}|}{hv_1}\int_{-\infty}^{0} dx\ \ Cos(2k_1x+\eta_1) + \frac{2|\tilde{r}_{22}|}{hv_2}\int_{-\infty}^{0} dx\ \ Cos(2k_2x+\eta_2) + \frac{1}{hv_1}\left(|t_{13}|^2+|t_{14}|^2+\cdots\right) + \frac{1}{hv_2}\left(|t_{23}|^2+|t_{24}|^2+\cdots\right)\right]$$

Now $|\tilde{r}_{11}|^2+|\tilde{r}_{21}|^2+|\tilde{t}_{11}|^2+|\tilde{t}_{21}|^2 = 1$

and $|\tilde{r}_{12}|^2+|\tilde{r}_{22}|^2+|\tilde{t}_{12}|^2+|\tilde{t}_{21}|^2 = 1$

Thus,

$$\rho(E) = \frac{2}{hv_1}\int_{-\infty}^{\infty} dx \;+\; \frac{2}{hv_2}\int_{-\infty}^{\infty} dx + \frac{2|\tilde{r}_{11}|}{hv_1}\int_{-\infty}^{\infty} dx\ \ Cos(2k_1x+\eta_1) + \frac{2|\tilde{r}_{22}|}{hv_2}\int_{-\infty}^{\infty} dx\ \ Cos(2k_2x+\eta_2) + \frac{2}{hv_1}\left(|t_{13}|^2+|t_{14}|^2+\cdots\right) + \frac{2}{hv_2}\left(t_{23}|^2+|t_{24}|^2+\cdots\right) \qquad \text{(iii)}$$

Now $\frac{2}{hv_1}\int_{-\infty}^{\infty} dx + \frac{2}{hv_2}\int_{-\infty}^{\infty} dx = \rho_0(E)$ i.e. DOS in the absence of scatterer. Also according to some text books [27], for plane wave states the current conservation condition

$$\frac{\partial}{\partial t}\int_{\Omega}\psi^*\psi\ \ d\tau \;+\; \int_S \vec{J}.\hat{n}\ \ ds \;=\; 0$$

can be satisfied if and only if the wave function vanishes at $\pm\infty$ for all energy. Thus the 3rd and 4th term of Eq.(iii) of this section is 0. Besides, neglecting these oscillatory terms in the leads is very standard in the derivation of Friedel sum rule [18], where it is assumed that the carrier concentration is so high in the leads that the leads are non-polarizable. However, assuming non-polarizable leads alone does not eradicate all energy dependence of the self energy as thought in Ref. [18] (see Eqs. 2 and 6 therein, the parameter t_α can be strongly energy dependent, which is dispersive behavior). So we get

$$\rho(E) = \rho_0(E) \;+\; \frac{2}{hv_1}\left(|t_{13}|^2 \;+\; |t_{14}|^2 \;+\cdots\right) + \frac{2}{hv_2}\left(|t_{23}|^2 \;+\; t_{24}|^2 \;+\cdots\right)$$

Thus $\rho(E) - \rho_0(E) = \frac{2}{hv_1}\left(|t_{13}|^2 \;+\; |t_{14}|^2 \;+\cdots\right) + \frac{2}{hv_2}\left(|t_{23}|^2 \;+\; t_{24}|^2 \;+\cdots\right) = (\rho-\rho_0)_R$

[1] R.G.Newton, Scattering theory of wave and particles (Springer - Verlag, New York, 1966), pg. 440.
[2] A.Yacoby et al., Phys. Rev. Lett. **74**, 4047 (1995)
[3] R. Schuster et al., Nature(London) **385**, 417 (1997)
[4] Cernicchiaro et. al, Phys. Rev. Lett. **79**, 273 (1997)
[5] P. Singha Deo, Phys. Rev.B **53**, 15447 (1996)
[6] In some cases these NSDN can lead to a spontaneously broken discrete symmetry like parity. P.Singha Deo et al., (to be published)
[7] A.J. Leggett, in Granular Nano-Electronics, Vol.251 of NATO Advanced Studies Institute, Series B: Physics, edited by D.K. Ferry, J.R. Barker and C. Jacoboni (Plenum, New York, 1991), p.297
[8] U.Fano Phys. Rev. **124**, 1866 (1961)
[9] P.F.Bagwell, Phys. Rev.B **41**, 10354(1990)
[10] E.Tekman and P.F.Bagwell Phys. Rev.B **48**, 2553 (1993); W. Porod, Z. Shao and C.S. Lent, Phys. Rev. B **48**, 8495 (1993).
[11] P. Singha Deo, Solid State Commun. **107**, 69 (1998)
[12] L.Yeyati and M.Büttiker, Phys. Rev.B **52**, R14360 (1995)
[13] P. Singha Deo and A.M.Jayannavar Mod. Phys. Lett. B **10**, 787 (1996)
[14] C.-Mo Ryu and S.Y.Cho, Phys. Rev.B **58**, 3587 (1998)
[15] H.Xu and W.Sheng, Phys. Rev.B **57**, 11903 (1998)
[16] H.W.Lee, Phys. Rev. Lett. **82**, 2358 (1999)
[17] T.Taniguchi and M.Buttiker, Phys. Rev.B **60**, 13814 (1999)
[18] A.L.Yeyati and M.Büttiker, Phys. Rev. B **62**, 7307 (2000).
[19] J.Friedel, Philos. Mag. **43**, 153 (1952); J.M. Ziman, Principles of the Theory of Solids, 2nd ed., Cambridge University Press, 1972.
[20] J.S.Langer and V.Ambegaokar, Phys. Rev. **121**, 1090 (1961)
[21] F.T.Smith Phys. Rev. **113**, 349 (1960)
[22] R. Landauer and T. Martin, Rev. Mod. Phys. **66**, 217 (1994).
[23] S.Griffith Trans. Faraday Soc. **49**, 650 (1953)
[24] P.S.Deo and A.M.Jayannavar Mod. Phys. Lett. **B 7**, 1045 (1993); P. Singha Deo and A. M. Jayannavar, cond-mat/0006035 and references therein.
[25] From the derivation of the FSR (one can see the book by Ziman in Ref. [19]), that the scattering phase shift is defined such that when we set the scattering potential to 0 the scattering phase shift is also 0. However, in the double delta function potential the $arg(t) = kl$ when the strength of the delta function potentials are set to zero. Hence the scattering phase shift is $arg(t) - kl$. However, the term coming from the derivative of kl cancels with the term coming from ρ_0, leading to the Eq. in (11).
[26] V. Gasperin, T. Christen and M. Büttiker, Phys. Rev. A **54**, 4022 (1996).
[27] Quantum Mechanics by A.K. Ghatak and S. Loknathan, third edition, Macmillan India Ltd., pg. 57.